1 Time-dependent propagation of a coin-shaped crack

In this section, the propagation of a coin-shaped (penny-shaped) crack in a three-dimensional viscoelastic solid is investigated using a cohesive-zone-based finite-element formulation. Crack growth is driven by stress relaxation under a prescribed external loading and is described as a sequence of quasi-static equilibrium states with an explicitly tracked crack front.

The analysis exploits symmetry and considers a quarter of the crack embedded in a cubic block. A locally refined finite-element mesh is introduced in an annular region surrounding the crack front, while coarser elements are used away from this zone. A cohesive interface with a finite process zone is embedded along the crack surface and governed by a smoothed trapezoidal traction–separation law.

1.1 Crack-growth criterion and control parameter

Crack propagation is controlled by a local opening condition evaluated at the current crack-front node. At each propagation step, the following criterion is enforced:

$$\frac{2u_z}{\Delta_{\max}} = k_D, \tag{1}$$

where u_z is the normal opening displacement at the active crack-front node, $\Delta_{\max}$ is the critical cohesive opening displacement, and $k_D \in (0, 1]$ is a prescribed damage parameter.

The parameter k_D is increased incrementally. Once $k_D = 1$ is reached, the crack front advances to the next node along the predefined crack path. This strategy provides a controlled and stable simulation of crack-front evolution without introducing ad hoc remeshing or heuristic growth rules. In the present implementation, the crack-front advance is realized by updating the active cohesive index (front node) and continuing the damage-controlled evolution for the next segment of the predefined front.

1.2 Determination of the physical time increment

A central aspect of the algorithm is the determination of the physical time increment corresponding to a prescribed external stress level. Instead of introducing an artificial time step, the increment Δt is computed implicitly from the nonlinear condition

$$\sigma_z(\Delta t) = \sigma^{\text{ext}}, \tag{2}$$

where σ^{ext} is the applied external stress and σ_z is the stress response at the crack front accounting for viscoelastic relaxation.

Equation (2) is solved using the MATLAB root-finding routine `fzero`. For a given trial value of Δt, the viscoelastic internal variables are updated analytically using exponential relaxation kernels, the tangent stiffness matrix is reconstructed, and the global equilibrium problem is solved. The resulting stress level is then compared with σ^{ext}, and the root of $\sigma_z(\Delta t) - \sigma^{\text{ext}} = 0$ is determined.

To ensure robustness, the root is bracketed automatically by scanning Δt over a small set of logarithmically spaced trial values. The first sign change of $g(\Delta t) = \sigma_z(\Delta t) - \sigma^{\text{ext}}$ defines a valid bracket interval for `fzero`. In the reported computations, this bracketing strategy resulted in stable convergence, with residuals reduced to machine precision and without sensitivity to the initial guess. Importantly, the computed Δt provides a physically meaningful time scale governed directly by the material relaxation properties.

1.3 Displacement and stress profiles at the crack surface

The evolution of the cohesive zone is conveniently illustrated through profiles along the crack surface. At each saved step, we plot the normalized crack opening $2u_z/\Delta_{\max}$ and the normalized normal stress $\sigma_z/\sigma_{\max}$ as functions of the radial coordinate x measured along the crack surface. The current crack radius R_c is indicated by the vertical dashed line.

A practical observation in three-dimensional cohesive simulations is that for shallow meshes the raw stress component σ_z may exhibit unphysical sign changes near the front due to discretization effects. To avoid misleading trends, we therefore present the *normalized* stress $\sigma_z/\sigma_{\max}$, which remains within $[0, 1]$ and enables consistent comparison between time steps.

Figure 1 summarizes ten steps for which the cohesive zone remains fully inside the refinement ring. The plots demonstrate: (i) a strong localization of the opening field near the crack front, (ii) a pronounced, smooth stress peak within the cohesive/process zone, and (iii) a systematic outward shift of the profiles as the crack advances.

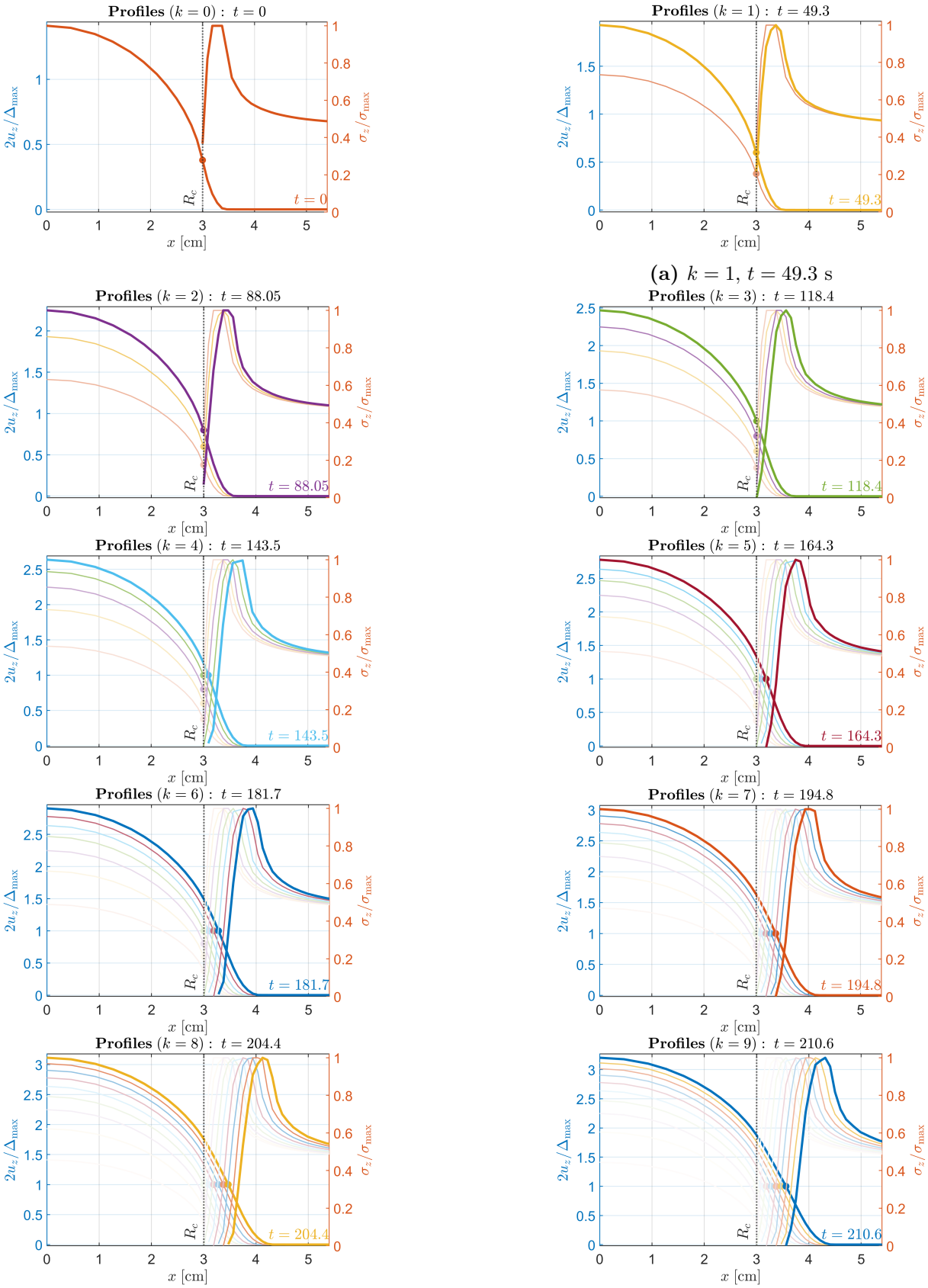

(a) $k = 1$, $t = 49.3$ s

Figure 1: Normalized cohesive profiles along the crack surface at ten successive steps while the cohesive/process zone remains inside the refinement ring. Each panel shows $2u_z/\Delta_{\max}$ and $\sigma_z/\sigma_{\max}$ versus x, with the current crack radius R_c marked by the vertical dashed line.

1.4 Time–radius relationship

The evolution of the crack radius $a(t)$ obtained from the proposed algorithm is shown in Fig. 2. An initial incubation stage with a stationary crack is followed by a phase of accelerated crack growth once the critical opening condition (1) is satisfied. This behavior emerges naturally from the coupled solution of the viscoelastic constitutive equations, the cohesive-zone model, and the implicit determination of the time increment. No additional assumptions regarding the crack-growth rate are introduced.

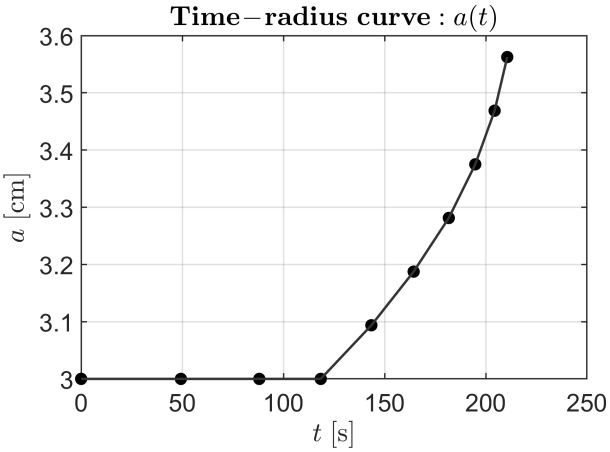

Figure 2: Time–radius curve $a(t)$ for the coin-shaped crack. The incubation stage (no growth) is followed by stable quasi-static propagation driven by viscoelastic relaxation under sustained loading.

For transparency, Table 1 summarizes the crack radius recorded at the ten saved steps. The crack remains at $a_0 = 3.0$ cm during the early part of the simulation and subsequently increases monotonically as the front advances in the refined ring.

Table 1: Recorded crack radius $a(t)$ at the saved steps corresponding to Fig. 1.

k	t [s]	$a(t)$ [cm]
0	0.0	3.0000
1	49.3	3.0000
2	88.1	3.0000
3	118.4	3.0000
4	143.5	3.0938
5	164.3	3.1875
6	181.7	3.2813
7	194.8	3.3750
8	204.4	3.4688
9	210.6	3.5625

1.5 Stress field near the crack front: initial, incubation, and growth stages

To visualize the spatial evolution of the fracture process zone, we plot the normalized stress field $\sigma_z/\sigma_{\max}$ at three characteristic time instants: (i) $t = 0$ s (initial), (ii) $t = 118.4$ s

(end of incubation), and (iii) $t = 210.6$ s (advanced growth). The results are shown in Fig. 3.

At $t = 0$ s, the stress concentration is localized near the initial crack front, and the cohesive annulus is confined to the refined ring. During the incubation stage, the crack radius remains unchanged; nevertheless, viscoelastic relaxation redistributes stresses in the vicinity of the front. At $t = 118.4$ s, the stress field indicates that the system approaches the critical configuration at which the cohesive condition (1) becomes active. Finally, at $t = 210.6$ s, the zone of elevated stresses has shifted outward consistently with the increased crack radius, demonstrating stable quasi-static propagation with a smooth stress gradient across the cohesive/process zone.

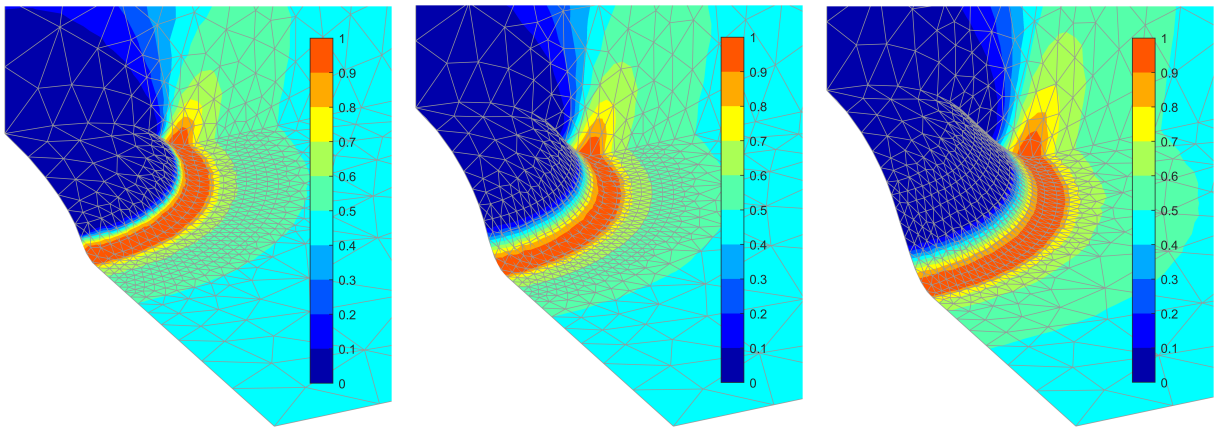

(a) $t = 0$ s **(b)** $t = 118.4$ s (incubation) **(c)** $t = 210.6$ s (growth)

Figure 3: Normalized stress field $\sigma_z/\sigma_{\max}$ near the crack front at three characteristic time instants: initial state, end of incubation, and advanced propagation. The annular zone of elevated stress tracks the crack edge, confirming consistent front evolution and adequate resolution of the cohesive process zone by the refinement ring.

Overall, the combined analysis of profiles (Fig. 1), the time–radius curve (Fig. 2), and the stress-field snapshots (Fig. 3) confirms that crack advance in the present problem is governed by a time-dependent mechanism: a delayed activation (incubation) followed by stable quasi-static propagation driven by viscoelastic relaxation under sustained loading.